

Electrolessly Deposited Electrospun Metal Nanowire Transparent Electrodes

Po-Chun Hsu,[†] Desheng Kong,[†] Shuang Wang,[‡] Haotian Wang,[§] Alex J. Welch,[†] Hui Wu,^{†,⊥} and Yi Cui^{*,†,||}

[†]Department of Materials Science and Engineering, [‡]Department of Electrical Engineering, and [§]Department of Applied Physics, Stanford University, Stanford, California 94305, United States

^{||}SLAC National Accelerator Laboratory, Stanford Institute for Materials and Energy Sciences, Menlo Park, California 94025, United States

S Supporting Information

ABSTRACT: Metal nanowire (MNW) transparent electrodes have been widely developed for their promising sheet resistance (R_s)–transmittance (T) performance, excellent mechanical flexibility, and facile synthesis. How to lower the junction resistance without compromising optical transmittance has become the key issue in enhancing their performance. Here we combine electrospinning and electroless deposition to synthesize interconnected, ultralong MNW networks. For both silver and copper nanowire networks, the R_s and T values reach around 10 Ω /sq and 90%, respectively. This process is scalable and takes place at ambient temperature and pressure, which opens new opportunities for flexible electronics and roll-to-roll large-scale manufacturing.

Transparent conducting electrodes (TCEs) are indispensable components in many optoelectronic devices such as displays, light-emitting diodes (LEDs), touchscreens, smart windows, and solar cells.¹ It is important to develop transparent electrodes with low sheet resistance (R_s) at high transmittance (T) to decrease the ohmic loss of the electronic circuit while maintaining good transparency. Currently the dominant material for TCE is indium tin oxide (ITO), but its high cost and brittleness limit its applications.² Various alternative TCEs are being developed such as conducting polymers,³ carbon nanotubes,⁴ graphenes,⁵ and metal nanowire (MNW) networks.⁶ Among these novel TCEs, MNW networks are particularly promising because of their high electrical conductivity; intensive research efforts have been focused on enhancing their R_s – T performance. Recently the mesoscale metal wire concept was combined with MNW networks to further reduce R_s by an order of magnitude.⁷ Key issues to address for MNW TCEs are junction resistance and the number of junctions that conducting pathways encounter.⁸ Junction resistance can be greatly decreased by post-treatments such as thermal annealing,^{6d} wet chemical coating,⁸ nanoplasmonic welding,⁹ and electrowelding,¹⁰ however, these often limit the use of substrates and increase the process complexity. To decrease the number of junctions, longer NWs must be synthesized: longer NWs not only require fewer junctions to reach the contact pad but also lower the percolation threshold N_c , expressed as $\sqrt{(\pi N_c)} = 4.236/L$,^{4c} where L is the length of NWs. It is clear that for longer

NWs, N_c is lower, and the probability of having a continuous pathway becomes higher, resulting in lower R_s . The best solution-processed MNW TCEs are reported to have R_s and T values of 9 Ω /sq and 89%, respectively, for silver nanowires (AgNWs)^{9b} and 40 Ω /sq and 90%, respectively, for copper nanowires (CuNWs).¹¹ Here, we propose a novel method to synthesize interconnected, ultralong, high-performance MNWs at ambient temperature and pressure, which is suitable for flexible and soft substrates. By using electrospinning and electroless deposition, we are able to solve both junction resistance and NW length issues. This approach produces MNWs that are low-cost and scalable but also have decent R_s – T performance.

The process flow of electrolessly deposited metallic electrospun NW TCEs is shown in Figure 1. Essentially, the electrospun

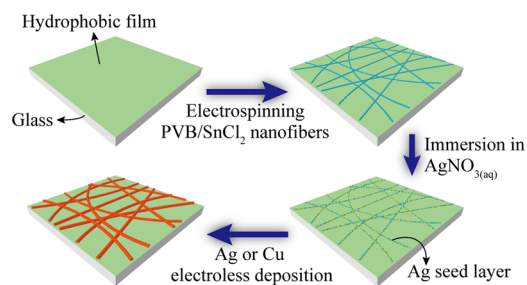


Figure 1. Schematic of electrolessly deposited metallic electrospun nanowire transparent electrodes. PVB/SnCl₂ NWs were electrospun onto a glass slide spin-coated with hydrophobic PVB thin film, followed by immersion into AgNO₃ solution to form an Ag catalyst seed layer. The sample was then rinsed and transferred to electroless deposition solution to form Ag or Cu NWs.

polyvinyl butyral (PVB) NWs network was used as the template for electroless metal deposition. Electrospinning produces ultralong NWs¹² that provide continuous pathways for electron transport after metallization of the NW network. Electroless deposition is a well-established technique for depositing metal films at low cost and large scale. In combination, these two methods offer a cost-effective way to make MNW networks. To guarantee great R_s – T performance, it is necessary to selectively deposit metal on the PVB NWs instead of the substrate. This

Received: June 12, 2014

Published: July 14, 2014

issue is tackled by two key steps in our method. First, tin(II) chloride is dissolved in the PVB solution, electrospun as PVB/SnCl₂ NWs. When the NWs are immersed in silver nitrate aqueous solution, Ag⁺ is reduced by Sn²⁺ and forms a Ag seed layer on the surface, which acts as the catalytic nucleation site for Ag or Cu electroless deposition.¹³ Second, the substrates are spin-coated with hydrophobic polymer film before the PVB nanofiber electrospinning, so it is more energetically unfavorable for metal precursors to be reduced onto the substrates. Here we also use PVB for the hydrophobic coating.

The electrospun PVB/SnCl₂ NWs are characterized by X-ray photoelectron spectroscopy (XPS) before and after AgNO₃ treatment (Figure 2a). For the as-electrospun NWs, the Sn 3d_{5/2} peak was deconvoluted and fitted as two subpeaks at 487.0 and 488.7 eV. According to previous XPS research,¹⁴ the lower binding energy subpeak (487.0 eV) corresponds to the SnCl₂

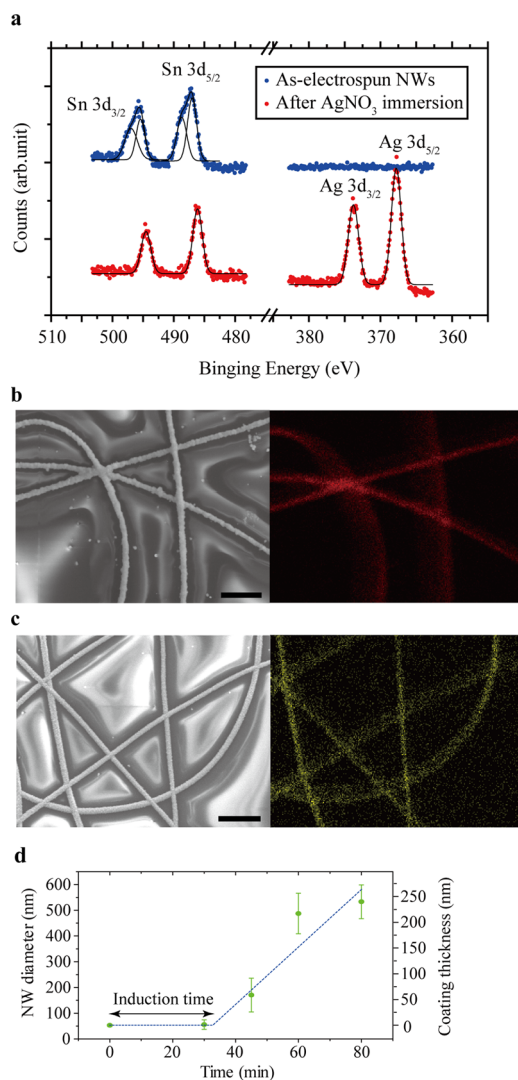


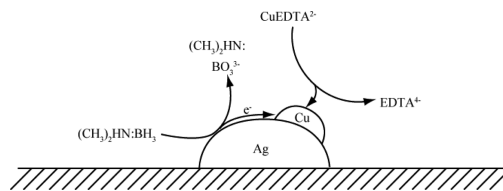
Figure 2. (a) XPS spectra of nanowires as-electrospun and after AgNO₃ treatment, referenced to C 1s at 284.5 eV. (b,c) SEM and EDS mapping of Ag and Cu NWs on glass substrates, respectively. The scale bars are 2 μm. Note that there is no conductive coating for imaging, so the substrates are insulating and cause charging effect between the NWs. (d) CuNW diameter vs electroless deposition time. The diameter of the electrospun PVB/SnCl₂ NWs is ~60 nm. The electroless deposition exhibits an induction time of ~30 min, followed by a constant-rate deposition. The blue dashed line is a guide.

dispersed in the NW, while the higher binding energy subpeak might correspond to SnO₂ or Sn(OH)₄ impurities due to oxidation of Sn²⁺ species when exposed to ambient atmosphere.¹⁵ After AgNO₃ treatment, Sn²⁺ is expected to be oxidized to Sn⁴⁺, and Ag seeds should appear and bind to the NW surface, as indicated by the Ag 3d_{5/2} peak. The XPS result again agrees very well with the literature,¹⁴ showing a 0.8 eV shift toward lower binding energy down to 486.2 eV for the Sn 3d_{5/2} peak. The XPS study supports the use of SnCl₂ and AgNO₃ as reagents to provide a Ag seed layer to catalyze the subsequent electroless deposition.

Systematic characterizations reveal the morphology and composition of the as-synthesized NW network. Figure 2b,c shows the scanning electron microscopy (SEM) image and the corresponding energy-dispersive spectroscopy (EDS) elemental map of electrolessly deposited AgNWs and CuNWs, respectively. The red color in the EDS represents AgL characteristic radiation, and green represents CuK. Apparently, the substrate passivated by hydrophobic coating is free of metal deposition, and the Ag seed catalysts successfully facilitate metallization on the polymer NWs. For TCE applications, the NWs used in our study are generally 200 nm in diameter. With the diameter of electrospun NWs being ~60 nm (Figure S1), the thickness of metal deposition is ~70 nm. We intentionally reduce the diameter of PVB NWs as much as possible, since the polymer cores of the NWs do not contribute to the electrical conductance. The thickness of MNWs must also be carefully chosen. Thin deposition gives smaller crystal grains and therefore more defects or voids, while thick deposition reduces the optical transmittance compared to the thin counterpart, given the same NW density. We found that a 70 nm thickness guarantees complete metallization coverage as well as high optical transmittance.

The time dependence of the thickness of CuNWs is shown in Figure 2d. The growth exhibits an induction period followed by a linear increase in the thickness. This behavior agrees well with the mixed-potential theory,¹⁶ in which the induction period is the duration until the reducing agent and the metal ions reach the same potential before deposition occurs. The chemical equations for Cu electroless deposition by dimethylamine borane (DMAB) are illustrated in Scheme 1.

Scheme 1. Copper Electroless Deposition in Alkaline Solution Using EDTA as Chelating Agent and DMAB as Reducing Agent



During the incubation period, the Ag catalyst seed layer facilitates oxidation of DMAB to reach the same potential as the metal precursors, and thus steady-state electroless deposition can occur. It is worth noting that the incubation time significantly depends on the atmosphere and stirring rate,¹⁷ so good control of the oxygen partial pressure and stirring environment is important to guarantee uniformity and reproducibility.

Figure 3a shows the R_s - T relationships of our electrolessly deposited MNWs, which are controlled by the electrospinning time and resulting NW areal density. To our knowledge, this R_s - T performance (8.5 Ω/sq and 90% for AgNWs, 11.2 Ω/sq and

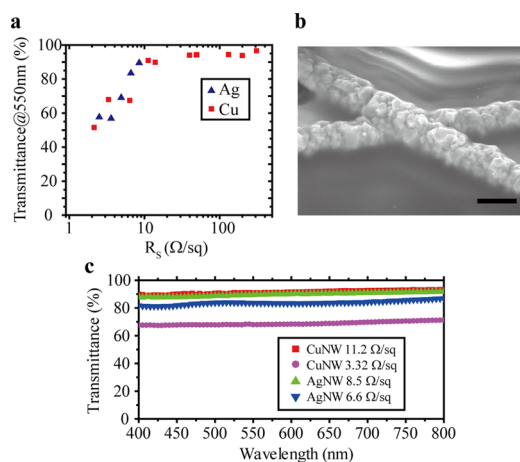


Figure 3. (a) R_s – T performance of electroless deposited nanowire transparent electrodes. Different R_s – T values correspond to different NW areal densities. These unprecedentedly high performances show that not only AgNWs but also low-cost CuNWs can work as an effective transparent electrodes. (b) 45° tilted-view SEM image of AgNWs. The electroless deposition covers and fuses the entire junction, explaining the high performance of the transparent electrode. The scale bar is 500 nm. (c) Transmittance spectra of electrolessly deposited metal NWs. The spectra are nearly the same from 350 to 800 nm, suggesting a large transmittance window for transparent electrode application.

91% for CuNWs) is so far the best reported for chemically synthesized MNW networks. This high performance is due to the reduced number of junctions and low junction resistances. As electrospinning can produce centimeter-long NWs,^{6h} ~100–1000 times longer than individual solution-processed MNWs,^{6d,9b} the percolation threshold and continuous charge transport pathway can be easily achieved. Moreover, the tilted-view SEM image in Figure 3b clearly shows the fused AgNW–AgNW junction. Because the metal deposition occurs after the polymer NW network forms, the metallization covers the NW surface and naturally “fuses” the junctions at the NW intersections, directly avoiding the typical high junction resistance for solution-processed MNW network TCEs. Further elevating the deposition temperature or optimizing the reducing/complexing conditions should reduce the resistivity of MNWs.¹⁶

We noted that the surface of our electrolessly deposited MNWs is rougher than those of ordinary solution-processed NWs due to its polycrystalline nature. Nevertheless, it is the NW diameter or the protrusion of NWs that contributes to the roughness, so the NW surface roughness is less critical. Plenty of reports deal with the roughness issue, including polymer embedding,¹⁸ mechanical pressing,¹⁹ graphene coating,²⁰ and sol–gel coating.²¹ All of these methods are perfectly applicable to our electrolessly deposited MNW TCEs, allowing the fabrication of high-performance organic electronic devices.

In addition to excellent electrical properties, MNW TCEs also exhibit a large and flat transmittance window (Figure 3c). In contrast to transparent conducting oxides, the transparency of MNWs is attributed to empty areas between NWs. All light that has wavelength shorter than the size of the empty areas can easily pass through. Since the size of these empty areas is usually larger than several μm or even tens of μm , the MNW TCEs allow a wide band of light to transmit, which can enhance the efficiency of optoelectronic devices such as photovoltaics, photodetectors, and LEDs.

Mechanical flexibility is a major advantage of MNW over metal oxide TCEs. Figure 4a shows a bending test of a CuNW network

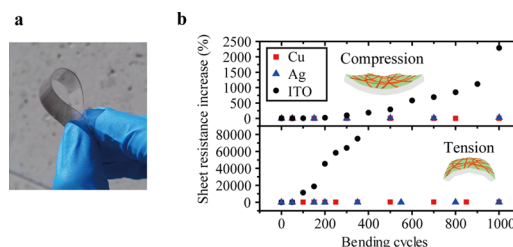


Figure 4. (a) Photograph of a copper nanowire transparent electrode deposited on a flexible PET substrate. (b) Percentage sheet resistance change after 1000 bending cycles. The bending radius is 4 mm. The metal nanowires exhibit superior flexibility compared to ITO counterparts.

coated on a polyethylene terephthalate (PET) substrate. To quantitatively demonstrate the flexibility and durability, the bending cycle test was performed up to 1000 cycles, with a bending radius of 4 mm (Figure 4b). The MNWs exhibit superior bending durability compared to ITO thin films under both compressive and tensile strain. For compressive bending, R_s of the ITO film increases 23 times after 1000 cycles, while that of MNWs increases only by a factor of 0.02–0.2. For tensile bending, R_s of ITO increases 1630 times after only 500 cycles, which is much faster than for compressive bending because of crack formation,²² while that of the MNWs only increases by 0.2–3.5 times. This dramatic difference in flexibility is because metal is intrinsically much more ductile than metal oxides, and nanostructures can also withstand a larger degree of bending. A MNW network composed of stacked individual NWs also achieved this level of flexibility in previous work;^{9b,23} however, annealing steps are usually required to reduce junction resistance, which can degrade the underlying plastic substrates for flexible electronic devices. For our electrolessly deposited MNWs, the junctions are already fused during the deposition, and the entire process is done at room temperature, so it has a much wider applicability and lower energy cost for flexible electronics.

Figure 5 demonstrates a large-scale CuNW TCE on an 11-cm-diameter polystyrene plate. Optical images taken at different locations on the CuNW network show that the wire density and diameter are uniform throughout the substrate. Considering that both electrospinning and electroless deposition can be readily scaled-up and are applicable to flexible substrates, our electroless

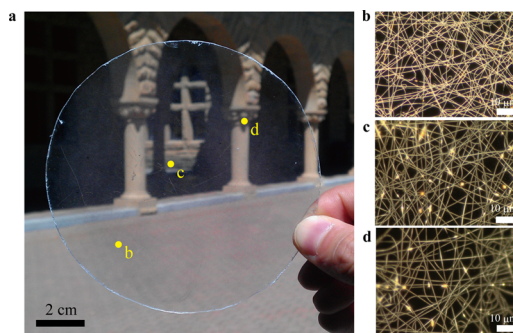


Figure 5. (a) Large-scale electrolessly deposited electrospun copper nanowire transparent electrode. (b–d) Optical images of various places on the sample, corresponding to the labeled points in (a), showing the uniformity of nanowire density and metal deposition.

deposition approach opens up the possibility of roll-to-roll processing, which is a great advantage for industrial fabrication.

The combination of electrospinning and electroless deposition to produce large-scale MNW mats has been demonstrated previously.²⁴ Park et al.^{24a} used a complexation/reduction cycle to selectively coat gold onto a polymer nanofiber mat, which also might be applied to prevent the metal from coating onto the transparent substrates. These reports show the scalability of our approach and the potential for making other MNWs, e.g., gold, nickel, or zinc.

To summarize, electroless deposition was used to synthesize silver and copper nanowire transparent conducting electrodes with electrospun polymer nanowires as the templates. This approach can produce junction-free metal nanowire networks, thus greatly enhancing the R_s - T performance. The entire process was carried out at ambient temperature and pressure, which is not only energy-efficient but also suitable for flexible substrates. The scalability of this method has also been demonstrated. We believe electrolessly deposited metal nanowire TCEs can provide new opportunities for the optoelectronics community.

■ ASSOCIATED CONTENT

Supporting Information

SEM images and experimental details. This material is available free of charge via the Internet at <http://pubs.acs.org>.

■ AUTHOR INFORMATION

Corresponding Author

yicui@stanford.edu

Present Address

[†]H. Wu: Department of Materials Science and Engineering, Tsinghua University, Beijing 100084, China

Notes

The authors declare no competing financial interest.

■ ACKNOWLEDGMENTS

This work was partially supported by the Center on Nanostructuring for Efficient Energy Conversion (CNEEC). P.-C.H. acknowledges funding support from an International Fulbright Science and Technology Fellowship.

■ REFERENCES

- (1) (a) Granqvist, C. G. *Sol. Energy Mater. Sol. C* **2007**, *91*, 1529. (b) Ellmer, K. *Nat. Photon.* **2012**, *6*, 808. (c) Facchetti, A.; Marks, T. J. *Transparent Electronics: From Synthesis to Applications*; Wiley: New York, 2010.
- (2) (a) U.S. Geological Survey. *Mineral Commodity Summaries*, 2013. (b) Hecht, D. S.; Hu, L. B.; Irvin, G. *Adv. Mater.* **2011**, *23*, 1482. (c) Hu, L. B.; Wu, H.; Cui, Y. *MRS Bull.* **2011**, *36*, 760.
- (3) Heeger, A. J. *MRS Bull.* **2001**, *26*, 900.
- (4) (a) Wu, Z. C.; Chen, Z. H.; Du, X.; Logan, J. M.; Sippel, J.; Nikolou, M.; Kamaras, K.; Reynolds, J. R.; Tanner, D. B.; Hebard, A. F.; Rinzler, A. G. *Science* **2004**, *305*, 1273. (b) Zhang, M.; Fang, S. L.; Zakhidov, A. A.; Lee, S. B.; Aliev, A. E.; Williams, C. D.; Atkinson, K. R.; Baughman, R. H. *Science* **2005**, *309*, 1215. (c) Hu, L.; Hecht, D. S.; Gruner, G. *Nano Lett.* **2004**, *4*, 2513. (d) Rowell, M. W.; Topinka, M. A.; McGehee, M. D.; Prall, H. J.; Dennler, G.; Sariciftci, N. S.; Hu, L. B.; Gruner, G. *Appl. Phys. Lett.* **2006**, *88*, No. 233506.
- (5) (a) Bae, S.; Kim, H.; Lee, Y.; Xu, X. F.; Park, J. S.; Zheng, Y.; Balakrishnan, J.; Lei, T.; Kim, H. R.; Song, Y. I.; Kim, Y. J.; Kim, K. S.; Ozyilmaz, B.; Ahn, J. H.; Hong, B. H.; Iijima, S. *Nat. Nanotechnol.* **2010**, *5*, 574. (b) Kim, K. S.; Zhao, Y.; Jang, H.; Lee, S. Y.; Kim, J. M.; Kim, K. S.; Ahn, J. H.; Kim, P.; Choi, J. Y.; Hong, B. H. *Nature* **2009**, *457*, 706.

(c) Li, X. L.; Zhang, G. Y.; Bai, X. D.; Sun, X. M.; Wang, X. R.; Wang, E.; Dai, H. J. *Nat. Nanotechnol.* **2008**, *3*, 538. (d) Wang, X.; Zhi, L. J.; Mullen, K. *Nano Lett.* **2008**, *8*, 323.

(6) (a) Soltanian, S.; Rahmanian, R.; Gholamkhash, B.; Kiasari, N. M.; Ko, F.; Servati, P. *Adv. Energy Mater.* **2013**, *3*, 1332. (b) Hsu, P. C.; Wu, H.; Carney, T. J.; McDowell, M. T.; Yang, Y.; Garnett, E. C.; Li, M.; Hu, L. B.; Cui, Y. *ACS Nano* **2012**, *6*, 5150. (c) Kang, M. G.; Kim, M. S.; Kim, J. S.; Guo, L. J. *Adv. Mater.* **2008**, *20*, 4408. (d) Lee, J. Y.; Connor, S. T.; Cui, Y.; Peumans, P. *Nano Lett.* **2008**, *8*, 689. (e) Li, H. P.; Pan, W.; Zhang, W.; Huang, S. Y.; Wu, H. *Adv. Funct. Mater.* **2013**, *23*, 209. (f) Rathmell, A. R.; Bergin, S. M.; Hua, Y. L.; Li, Z. Y.; Wiley, B. J. *Adv. Mater.* **2010**, *22*, 3558. (g) Wu, H.; Hu, L. B.; Rowell, M. W.; Kong, D. S.; Cha, J. J.; McDonough, J. R.; Zhu, J.; Yang, Y. A.; McGehee, M. D.; Cui, Y. *Nano Lett.* **2010**, *10*, 4242. (h) Wu, H.; Kong, D. S.; Ruan, Z. C.; Hsu, P. C.; Wang, S.; Yu, Z. F.; Carney, T. J.; Hu, L. B.; Fan, S. H.; Cui, Y. *Nat. Nanotechnol.* **2013**, *8*, 421. (i) Kang, M. G.; Xu, T.; Park, H. J.; Luo, X. G.; Guo, L. J. *Adv. Mater.* **2010**, *22*, 4378. (j) Azuma, K.; Sakajiri, K.; Matsumoto, H.; Kang, S. M.; Watanabe, J.; Tokita, M. *Mater. Lett.* **2014**, *115*, 187. (k) Gao, T. C.; Wang, B. M.; Ding, B.; Lee, J. K.; Leu, P. W. *Nano Lett.* **2014**, *14*, 2105.

(7) Hsu, P. C.; Wang, S.; Wu, H.; Narasimhan, V. K.; Kong, D. S.; Lee, H. R.; Cui, Y. *Nat. Commun.* **2013**, *4*, 2522.

(8) Hu, L. B.; Kim, H. S.; Lee, J. Y.; Peumans, P.; Cui, Y. *ACS Nano* **2010**, *4*, 2955.

(9) (a) Garnett, E. C.; Cai, W. S.; Cha, J. J.; Mahmood, F.; Connor, S. T.; Christoforo, M. G.; Cui, Y.; McGehee, M. D.; Brongersma, M. L. *Nat. Mater.* **2012**, *11*, 241. (b) Lee, J.; Lee, P.; Lee, H.; Lee, D.; Lee, S. S.; Ko, S. H. *Nanoscale* **2012**, *4*, 6408.

(10) Song, T. B.; Chen, Y.; Chung, C. H.; Yang, Y.; Bob, B.; Duan, H. S.; Li, G.; Tu, K. N.; Huang, Y.; Yang, Y. *ACS Nano* **2014**, *8*, 2804.

(11) Ye, S. R.; Rathmell, A. R.; Stewart, I. E.; Ha, Y. C.; Wilson, A. R.; Chen, Z. F.; Wiley, B. J. *Chem. Commun.* **2014**, *50*, 2562.

(12) Li, D.; Xia, Y. N. *Adv. Mater.* **2004**, *16*, 1151.

(13) Lee, C. L.; Syu, C. C. *Electrochim. Acta* **2011**, *56*, 8880.

(14) Pederson, L. R. *Sol. Energy Mater.* **1982**, *6*, 221.

(15) Wagner, C. D.; Gale, L. H.; Raymond, R. H. *Anal. Chem.* **1979**, *51*, 466.

(16) Schlesinger, M.; Paunovic, M. *Modern Electroplating*, 5th ed.; Wiley: New York, 2010.

(17) Dumesic, J.; Koutsky, J. A.; Chapman, T. W. *J. Electrochem. Soc.* **1974**, *121*, 1405.

(18) Yu, Z. B.; Zhang, Q. W.; Li, L.; Chen, Q.; Niu, X. F.; Liu, J.; Pei, Q. B. *Adv. Mater.* **2011**, *23*, 664.

(19) (a) Gaynor, W.; Burkhard, G. F.; McGehee, M. D.; Peumans, P. *Adv. Mater.* **2011**, *23*, 2905. (b) Hauger, T. C.; Al-Rafia, S. M. I.; Buriak, J. M. *ACS Appl. Mater. Inter.* **2013**, *5*, 12663.

(20) (a) Liu, Y.; Chang, Q. H.; Huang, L. J. *Mater. Chem. C* **2013**, *1*, 2970. (b) Lee, D.; Lee, H.; Ahn, Y.; Jeong, Y.; Lee, D. Y.; Lee, Y. *Nanoscale* **2013**, *5*, 7750.

(21) Zhu, R.; Chung, C. H.; Cha, K. C.; Yang, W. B.; Zheng, Y. B.; Zhou, H. P.; Song, T. B.; Chen, C. C.; Weiss, P. S.; Li, G.; Yang, Y. *ACS Nano* **2011**, *5*, 9877.

(22) Cairns, D. R.; Witte, R. P.; Sparacin, D. K.; Sachsman, S. M.; Paine, D. C.; Crawford, G. P.; Newton, R. R. *Appl. Phys. Lett.* **2000**, *76*, 1425.

(23) (a) Chung, C. H.; Song, T. B.; Bob, B.; Zhu, R.; Yang, Y. *Nano Res.* **2012**, *5*, 805. (b) Lee, M. S.; Lee, K.; Kim, S. Y.; Lee, H.; Park, J.; Choi, K. H.; Kim, H. K.; Kim, D. G.; Lee, D. Y.; Nam, S.; Park, J. U. *Nano Lett.* **2013**, *13*, 2814. (c) Guo, H. Z.; Lin, N.; Chen, Y. Z.; Wang, Z. W.; Xie, Q. S.; Zheng, T. C.; Gao, N.; Li, S. P.; Kang, J. Y.; Cai, D. J.; Peng, D. L. *Sci. Rep.* **2013**, *3*, No. 2323.

(24) (a) Park, M.; Im, J.; Park, J.; Jeong, U. *ACS Appl. Mater. Interfaces* **2013**, *5*, 8766. (b) Tao, D.; Wei, Q. F.; Cai, Y. B.; Xu, Q. X.; Sun, L. Y. *J. Coat. Technol. Res.* **2008**, *5*, 399. (c) Ochanda, F.; Jones, W. E. *Langmuir* **2005**, *21*, 10791.